

Adaptive Width Neural Networks

Federico Errica¹ Henrik Christiansen¹ Viktor Zaverkin¹ Mathias Niepert^{1,2} Francesco Alesiani¹

Abstract

For almost 70 years, researchers have mostly relied on hyper-parameter tuning to pick the width of neural networks’ layers out of many possible choices. This paper challenges the status quo by introducing an easy-to-use technique to learn an *unbounded* width of a neural network’s layer *during training*. The technique does not rely on alternate optimization nor hand-crafted gradient heuristics; rather, it jointly optimizes the width and the parameters of each layer via simple back-propagation. We apply the technique to a broad range of data domains such as tables, images, texts, and graphs, showing how the width adapts to the task’s difficulty. By imposing a soft ordering of importance among neurons, it is possible to *truncate* the trained network at virtually zero cost, achieving a smooth trade-off between performance and compute resources in a structured way. Alternatively, one can dynamically compress the network with no performance degradation. In light of recent foundation models trained on large datasets, believed to require billions of parameters and where hyper-parameter tuning is unfeasible due to huge training costs, our approach stands as a viable alternative for width learning.

1. Introduction

Since the construction of the Mark I Perceptron machine (Rosenblatt, 1958) the effective training of neural networks has remained an open research problem of great academic and practical value. The Mark I solved image recognition tasks by exploiting a layer of 512 *fixed* “association units” that in modern language correspond to the hidden units of a (possibly) Multi-Layer Perceptron (MLP). MLPs possess universal approximation capabilities when assuming *arbitrary width* (Cybenko, 1989) and sigmoidal activations, and their convergence to good solutions was studied, for instance, in Rumelhart et al. (1986) where the backpropaga-

¹NEC ²University of Stuttgart. Correspondence to: Federico Errica <federico.errica@neclab.eu>.

Preliminary work.

tion algorithm was described as “simple, easy to implement on parallel hardware”, and improvable by other techniques such as momentum that preserve locality of weight updates.

Yet, after almost 70 years of progress (LeCun et al., 2015), the vast majority of neural networks, be they shallow or deep, still rely on a fixed choice of the number of neurons in their hidden layers. This property is typically treated as an architectural design choice, one of the many hyper-parameters that have to be carefully tuned whenever we approach a new task (Wolpert, 1996). The tuning process has many names, such as model selection, hyper-parameter tuning, and cross-validation, and it is associated with non-negligible costs: Different architectural configurations are to be trained until one that performs best on a validation set is selected (Mitchell, 1997). The configurations’ space grows exponentially in the number of layers, so practitioners often resort to shortcuts such as picking a specific number of hidden units for *all* layers, which greatly reduces the search space together with the chances of selecting a better architecture for the task. Other techniques to tune hyper-parameters include constructive approaches (Fahlman & Lebiere, 1989; Wu et al., 2020), which alternate parameter optimization and creation of new neurons, natural gradient-based heuristics that dynamically modify the network (Mitchell et al., 2023), bi-level optimization (Franceschi et al., 2018), and neural architecture search (White et al., 2023), which often requires separate training runs for each configuration.

The hyper-parameters’ space exploration problem is exacerbated by the steep increase in size of recent neural architectures for language (Brown et al., 2020) and vision (Zhai et al., 2022), for example, where parameters are in the order of billions to (supposedly) accommodate for a huge dataset. Training these models requires an amount of time, compute power, and energy that currently makes it unfeasible for most institutions to perform a thorough model selection and find good width parameters; the commonly accepted compromise is to stick to previously successful hyper-parameter choices. This may also explain why network pruning (Blalock et al., 2020; Mishra et al., 2021), distillation (Zhang et al., 2019) and quantization (Mishra et al., 2021) techniques have recently been in the spotlight, as they trade-off hardware requirements and performance.

This work introduces a *simple* and *easy to use* technique to

learn the width of each neural network’s layer without imposing upper bounds (we refer to it as **unbounded width**). The width of each layer is *dynamically* adjusted during back-propagation using the latest deep learning libraries (Paszke et al., 2017), and it only requires a slight modification to the neural activations that does not alter the ability to parallelize computation. The technical strategy is to impose a soft ordering of hidden units by exploiting any monotonically decreasing function with unbounded support on natural numbers, which has a number of benefits. For instance, we do not need to fix a maximum number of neurons, which is typical of orthogonal approaches like supernet-works (White et al., 2023). As a by-product, we can achieve a straightforward trade-off between parametrization and performance by removing the last rows/columns of weight matrices, which corresponds to ignoring the “least important” neurons in the computation. Finally, we break symmetries in the parametrization of neural networks: it is not possible anymore to obtain an equivalent neural network behavior by permuting the weight matrices, which should in principle reduce the “jostling” effect where symmetric parametrizations compete at the beginning of training (Barber, 2012).

We test the proposed method on an MLP for tabular data, a Convolutional Neural Networks (CNN) (LeCun et al., 1989) for images, a Transformer architecture (Vaswani et al., 2017) for text, and a Deep Graph Network (DGN) (Micheli, 2009; Scarselli et al., 2009) for graphs, to showcase a broad scope of applicability. Empirical results suggest, as may be expected, that the width adapts to the task’s difficulty with the same performance of a fixed-width baseline. We investigate compressing of the network at training time while preserving accuracy, as well as a post-hoc truncation inducing a controlled trade-off at zero additional cost. Ablations suggest that the learned width is not influenced by the starting width (under bounded activations) nor by the batch size, advocating for a potentially large reduction of the hyper-parameter configuration space at model selection time.

2. Related Work

Constructive methods dynamically learn the width of neural networks and are related in spirit to this work. The cascade correlation algorithm (Fahlman & Lebiere, 1989) alternates standard training with the creation of a new hidden unit minimizing the neural network’s residual error. Similarly, the firefly network descent (Wu et al., 2020) grows the width and depth of a network every N training epochs via gradient descent on a dedicated loss. Yoon et al. (2018) propose an ad-hoc algorithm for lifelong learning that grows the network by splitting and duplicating units to learn new tasks. Wu et al. (2019) alternate training the network and then splitting existing neurons into offspring with equal weights. These works mostly focus on growing the neural

network; Mitchell et al. (2023) propose natural gradient-based heuristics to grow/shrink layers and hidden units of MLPs and CNNs. The main difference from our work is that we grow and shrink the network by simply computing the gradient of the loss, without relying on human-defined heuristics. The unbounded depth network of Nazaret & Blei (2022), from which we draw inspiration, learns the number of layers of neural networks. Compared to that work, we focus our attention to the number of neurons, modifying the internals of the architecture rather than instantiating a multi-output one. Finally, we mention Bayesian nonparametrics approaches (Orbanz & Teh, 2010) that learn a potentially infinite number of clusters in an unsupervised fashion.

Orthogonal Methods Neural Architecture Search (NAS) is an automated process that designs neural networks for a given task (Elsken et al., 2019b; White et al., 2023) and has been applied to different contexts (Zoph et al., 2018; Liu et al., 2019; So et al., 2019). Typically, neural network elements are added, removed, or modified based on validation performance (Elsken et al., 2019a; White et al., 2021; 2023), by means of reinforcement learning (Zoph & Le, 2016), evolutionary algorithms (Real et al., 2019), and gradient-based approaches (Liu et al., 2019). Typical NAS methods require enormous computational resources, sometimes reaching thousands of GPU days (Zoph & Le, 2016), due to the retraining of each new configuration. While recent advances on one-shot NAS models (Brock et al., 2018; Pham et al., 2018; Bender et al., 2018) have drastically reduced the computational costs, they mostly focus on CNNs, assume a bounded search space, and do not learn the width. As such, NAS methods are complementary to our approach. Bi-level optimization algorithms have also been used for hyper-parameter tuning (Franceschi et al., 2018), where hyper-parameters are the variables of the outer objective and the model parameters those of the inner objective. The solution sets of the inner problem are usually not available in closed form, which has been partly addressed by repeated application of (stochastic) gradient descent (Domke, 2012; Maclaurin et al., 2015; Franceschi et al., 2017). These methods are restricted to continuous hyper-parameters’ optimization, and cannot therefore be applied to width optimization. Finally, pruning (Blalock et al., 2020) and distillation (Hinton et al., 2015) are two methods that (only) reduce the size of neural networks by trading-off performances; the former deletes neural connections (Mishra et al., 2021) or entire neurons (Valerio et al., 2022; Dufort-Labbé et al., 2024), the latter trains a smaller network (student) to mimic a larger one (teacher) (Gou et al., 2021). Compared to most pruning approaches, our work can delete connections *and* reduce the model’s memory; compared to distillation, we do not necessarily need a new training. These techniques, however, can be easily combined with our approach.

3. Adaptive Width Learning

We introduce a general probabilistic framework, called Adaptive Width Neural Networks (AWNN) for convenience, showing how (ultimately simple) design choices arise from a variational inference treatment of a graphical model. We are given a dataset of N *i.i.d.* samples (x_i, y_i) , with input $x_i \in \mathbb{R}^F$, $F \in \mathbb{N}^+$ and target y_i whose domain depends on whether the task is regression or classification. The learning objective is to maximize

$$\log \prod_{i=1}^N p(y_i|x_i) = \sum_{i=1}^N \log p(y_i|x_i) \quad (1)$$

with respect to the learnable parameters of $p(y|x)$. To formalize learning of an MLP¹ that maximizes Equation (1) and **learns** an unbounded width for each hidden layer ℓ , we assume the existence of an **infinite** sequence of *i.i.d.* latent variables $\theta_\ell = \{\theta_{\ell n}\}_{n=1}^\infty$, where $\theta_{\ell n}$ is a multivariate variable over the learnable weights of neuron n at layer ℓ . Since this implies modeling an infinite-width layer, we introduce a latent variable λ_ℓ that decides how many neurons to use at each layer ℓ . That is, it “truncates” an infinite width to a **finite** value so that we can perform inference. For a network of L layers, we define $\theta = \{\theta_\ell\}_{\ell=1}^L$ and $\lambda = \{\lambda_\ell\}_{\ell=1}^L$, assuming independence across layers. Therefore, one can write $p(y_i|x_i) = \int p(y_i|\lambda, \theta|x_i) d\lambda d\theta$. Figure 1 (left) describes our independence assumptions of the generative model, which decompose the joint distribution as:

$$p(y_i, \lambda, \theta|x_i) = p(y_i|\lambda, \theta, x_i)p(\lambda)p(\theta) \quad (2)$$

$$p(\lambda) = \prod_{\ell=1}^L p(\lambda_\ell) = \prod_{\ell=1}^L \mathcal{N}(\lambda_\ell; \mu_\ell^\lambda, \sigma_\ell^\lambda) \quad (3)$$

$$p(\theta) = \prod_{\ell=1}^L \prod_{n=1}^\infty p(\theta_{\ell n}) = \prod_{\ell=1}^L \prod_{n=1}^\infty \mathcal{N}(\theta_{\ell n}; \mathbf{0}, \text{diag}(\sigma_\ell^\theta)) \quad (4)$$

$$p(y_i|\lambda, \theta, x_i) = \text{Neural Network of Section 3.1.} \quad (5)$$

Here, $\sigma_\ell^\theta, \mu_\ell^\lambda, \sigma_\ell^\lambda$ are hyper-parameters. The MLP is parametrized by realizations λ, θ , so it relies on a finite number of neurons and outputs either class probabilities (classification) or the mean of a Gaussian distribution (regression) to parametrize $p(y_i|\lambda, \theta, x_i)$ depending on the task. Maximizing Equation (1), however, requires computing the above integral, which is intractable. Therefore, we turn to mean-field variational inference (Jordan et al., 1999; Blei et al., 2017) to maximize an expected lower bound (ELBO) instead. This requires to define a distribution over the latent variables $q(\lambda, \theta)$ and re-phrase the objective as:

$$\sum_{i=1}^N \log p(y_i|x_i) \geq \sum_{i=1}^N \mathbb{E}_{q(\lambda, \theta)} \left[\log \frac{p(y_i|\lambda, \theta|x_i)}{q(\lambda, \theta)} \right], \quad (6)$$

¹Section 3.3 discusses extensions to other architectures.

where $q(\lambda, \theta)$ is parametrized by learnable *variational* parameters. We factorize the variational distribution into:

$$q(\lambda, \theta) = q(\lambda)q(\theta|\lambda) \quad (7)$$

$$q(\lambda) = \prod_{\ell=1}^L q(\lambda_\ell) = \prod_{\ell=1}^L \mathcal{N}(\lambda_\ell; \nu_\ell, 1) \quad (8)$$

$$q(\theta|\lambda) = \prod_{\ell=1}^L \prod_{n=1}^{D_\ell} q(\theta_{\ell n}) \prod_{n=D_\ell+1}^\infty p(\theta_{\ell n}) \quad (9)$$

$$q(\theta_{\ell n}) = \mathcal{N}(\theta_{\ell n}; \text{diag}(\rho_{\ell n}), \mathbf{I}). \quad (10)$$

$$D_\ell = \text{quantile function of } f_\ell(\cdot; \lambda_\ell) \text{ evaluated at } k \quad (11)$$

The value k is a hyper-parameter, $\nu_\ell, \rho_{\ell n}$ are variational parameters and, as before, we define $\rho_\ell = \{\rho_{\ell n}\}_{n=1}^{D_\ell}$, $\rho = \{\rho_\ell\}_{\ell=1}^L$ and $\nu = \{\nu_\ell\}_{\ell=1}^L$. Note that the set of variational parameters is **finite**. The **truncated width** D_ℓ , that is the finite number of neurons at layer ℓ , is computed as the quantile function evaluated at k of a distribution² f_ℓ with infinite support over \mathbb{N}^+ , parametrized by λ_ℓ . *W.l.o.g.*, we implement f_ℓ as a discretized exponential distribution, following the discretization strategy of Roy (2003): For every natural x , the discretized distribution relies on the cumulative distribution function (*c.d.f.*) of the exponential:

$$f_\ell(x; \lambda_\ell) = (1 - e^{\lambda_\ell(x+1)}) - (1 - e^{\lambda_\ell(x)}). \quad (12)$$

We choose the exponential because it is a **monotonically decreasing** function and allows us to impose an ordering of importance among neurons, as detailed in Section 3.1.

By expanding Equation 6 using the above definitions and approximating the expectations at the first order, *i.e.*, $\mathbb{E}_{q(\lambda)}[f(\lambda)] = f(\nu)$ and $\mathbb{E}_{q(\theta|\lambda)}[f(\theta)] = f(\rho)$ as in Nazaret & Blei (2022), we obtain the final form of the objective:

$$\begin{aligned} & \sum_{\ell=1}^L \log \frac{p(\nu_\ell; \mu_\ell^\lambda, \sigma_\ell^\lambda)}{q(\nu_\ell; \nu_\ell)} + \sum_{\ell=1}^L \sum_{n=1}^{D_\ell} \log \frac{p(\rho_{\ell n}; \sigma_\ell^\theta)}{q(\rho_{\ell n}; \rho_{\ell n})} + \\ & + \sum_{i=1}^N \log p(y_i|\lambda=\nu, \theta=\rho, x_i), \end{aligned} \quad (13)$$

where distributions’ parameters are made explicit to distinguish them. The first two terms in the loss regularize the width of the layers and the magnitude of the parameters, respectively, whereas the third is the predictive loss.

In practice, the finite variational parameters ν, ρ are those used by the neural network in place of λ, θ , which enables easy optimization via backpropagation. Maximizing Equation (13) will change each variational parameter ν_ℓ , which in turn will change the value of D_ℓ **during training**. If D_ℓ increases we initialize new neurons and draw their weights from a standard normal distribution, otherwise we remove

²General functions are allowed if a threshold can be computed.

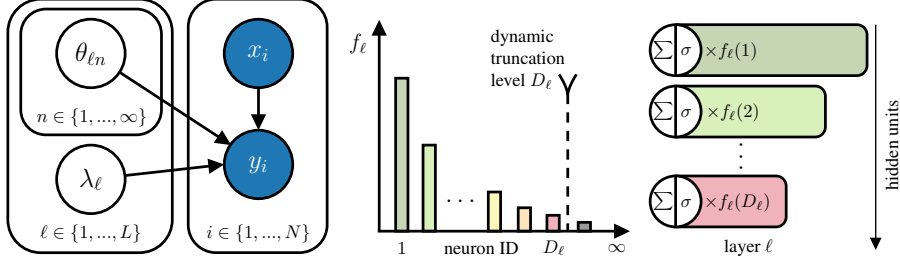


Figure 1. (Left) We depict the graphical model of AWNN, where observable random variables are dark and latent ones are white. (Middle) The distribution f_ℓ over hidden units’ importance at layer ℓ is parametrized by λ_ℓ . The width of layer ℓ is chosen as the quantile function of the distribution f_ℓ evaluated at k and denoted by D_ℓ . (Right) The hidden units’ activations at layer ℓ are rescaled by their importance.

the excess ones. When implementing mini-batch training, the predictive loss needs to be rescaled by N/M , where M is the mini-batch size. From a Bayesian perspective, this means regularizers weigh less if we have more data.

Compared to a fixed-width network with weight decay, we need to choose the values of $\mu_\ell^\lambda, \sigma_\ell^\lambda$, as well as initialize ν_ℓ (shared across layers as there is no particular reason to do otherwise). Therefore, we have two more hyper-parameters compared to the fixed-width network, but we make some considerations: **i**) it is always possible to use an uninformative prior over λ_ℓ , removing the extra hyper-parameters letting the model freely adapt the width of each layer (as is typical of frequentist approaches); **ii**) the choice of higher level of hyper-parameters is known to be less stringent than that of hyper-parameters themselves (Goel & Degroot, 1981; Bernardo & Smith, 2009), so we do not need to explore many values of μ_ℓ^λ and σ_ℓ^λ ; **iii**) our experiments suggest that AWNN converges to similar widths regardless of the starting point ν_ℓ , so that we may just need to perform model selection over one/two sensible initial values.

3.1. Imposing a Soft Ordering on Neurons’ Importance

Now that the learning objective has been formalized, the missing ingredient is the definition of the neural network $p(y_i | \lambda=\nu, \theta=\rho, x_i)$. Compared to a standard MLP, we need to make use of the variational parameters ν that affect the truncation width at each hidden layer, whereas ρ corresponds to the the usual MLP weights. We choose a monotonically decreasing function f_ℓ for the simple reason that when a new neuron is added, its relative importance is low and will not drastically impact the network. As a result, we are imposing a soft ordering of importance among neurons.

We modify the classical activation h_j^ℓ of a hidden neuron j at layer ℓ as

$$h_j^\ell = \sigma \left(\sum_{k=1}^{D_{\ell-1}} w_{jk}^\ell h_k^{\ell-1} \right) f_\ell(j; \nu_\ell), \quad (14)$$

where $D_{\ell-1}$ is the truncated width of the previous layer, σ is

a non-linear activation function and $w_{jk}^\ell \in \rho_{\ell j}$. That is, we rescale the activation of each neuron k by its “importance” $f_\ell(j; \nu_\ell)$. Note that the bias parameter is taken into account by concatenating a dummy value 1 to $h_k^{\ell-1}$.

It is easy to see that, in theory, the optimization algorithm could rescale the weights of the next layer by a factor $1/f_\ell(j; \nu_\ell)$ to compensate for the term $f_\ell(j; \nu_\ell)$. This may lead to a degenerate situation, which is actually quite common in classical MLPs, where the activations of the first neurons are small relative to the others, thus breaking the soft-ordering and wasting neurons. There are two strategies to address this undesirable effect. The first is to regularize the magnitude of the weights thanks to the prior $p(\theta_{\ell+1n})$, so that it may be difficult to compensate for the least important neurons that have a high $1/f_\ell(j)$. The second and less obvious strategy is to prevent the units’ activations of the current layer to compensate for high values by bounding their range. We apply both strategies to our experiments.

3.2. Rescaled Weight Initialization for Deep AWNN

Rescaling the activations of hidden units using Equation 14 causes activations of deeper layers to quickly decay to zero, as shown in Figure 2 for a 5-layer AWNN MLP with ReLU nonlinearity initialized using the well known kaiming scheme (He et al., 2015). This affects convergence since gradients get close to zero and it becomes impractical to train deep AWNN MLPs. We therefore derive a rescaled kaiming weight that guarantees that the variance of activation across layers is constant at initialization.

Theorem 3.1. *Let us consider an MLP with activations as in Equation 14 and ReLU nonlinearity. At initialization, given $\alpha_j^\ell = \sigma \left(\sum_{k=1}^{D_{\ell-1}} w_{jk}^\ell h_k^{\ell-1} \right)$*

$$\text{Var}[w_{j*}^\ell] = \frac{2}{\sum_{j=1}^{D_{\ell-1}} f_\ell^2(j)} \Rightarrow \text{Var}[\alpha_j^\ell] \approx \text{Var}[\alpha_j^{\ell-1}] \quad (15)$$

Proof. See Appendix A for an extended proof. \square

The extended proof shows there is a connection between the

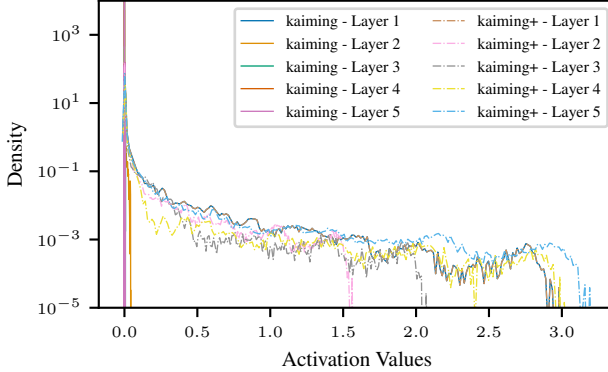


Figure 2. Effect of the rescaled initialization scheme (“kaiming+”) on a ReLU-based AWNN MLP, where neurons’ activations are computed using Equation 14. Compared to the standard initialization, the variance of activations agrees with the theoretical result.

variance of activations and the variance of gradients. In particular, the sufficient conditions over $\text{Var}[w_{j*}^\ell]$ are identical if one initializes all ν_ℓ in the same way for all layers. Therefore, if we initialize weights from a Gaussian distribution with standard deviation $\frac{\sqrt{2}}{\sqrt{\sum_{j=1}^{\ell-1} f_\ell^2(j)}}$, we guarantee that at initialization the variance of the deep network’s gradients will be constant. The effect of the new initialization (dubbed “kaiming+”) can be seen in Figure 2, where the distribution of activation values at initialization does not collapse in subsequent layers. This change drastically impacts overall convergence on the SpiralHard synthetic dataset (described in Section 4), where it appears it would be otherwise hard to converge using a standard kaiming initialization (please refer to Appendix A for a visual example).

Algorithm 1 summarizes the main changes to the training procedure, namely the new initialization and the update of the model’s truncated width at each training step.

3.3. Future Directions and Limitations

MLPs are ubiquitous in modern deep architectures. They are used at the very end of CNNs, in each encoder and decoder layer of Transformer, and they process messages coming from neighbors in DGNs. Our experiments focus on MLPs to showcase AWNN’s broad applicability, but there are many other scenarios where one can apply AWNN’s principles. For instance, one could impose a soft ordering of importance on CNNs’ filters at each layer, therefore learning the number of filters during training. Alternatively, one could investigate the application of AWNN to timeseries, since recurrent networks (Hochreiter & Schmidhuber, 1997) can be seen as a special case of an MLP with weight sharing. From a more theoretical perspective, we believe one could draw connections between our technique and the Information Bottleneck principle (Tishby et al., 2000), which seeks

Algorithm 1 AWNN Training Procedure

```

1: Input: Dataset  $\mathcal{D}$ , initialized AWNN model  $\mathcal{M}$  (Section 3.2)
2: Output: Trained AWNN Model  $\mathcal{M}$ 
3: for each training epoch do
4:   for batch in  $\mathcal{D}$  do
5:     update_width( $\mathcal{M}$ )
6:      $\hat{y} \leftarrow \mathcal{M}(\text{batch})$ 
7:     loss  $\leftarrow \text{ELBO}(\mathcal{M}, \text{batch}, \hat{y})$  // Eq. 13
8:      $\mathcal{M} \leftarrow \text{backpropagation}(\mathcal{M}, \text{loss})$ 
9:   function update_width( $\mathcal{M}$ ):
10:    for layer  $\ell$  in  $\mathcal{M}.\text{hidden\_layers}$  do
11:       $D_\ell \leftarrow \text{quantile function of } f_\ell(\cdot; \nu_\ell) \text{ evaluated at } k$ 
12:      Use  $D_\ell$  to update  $\rho_\ell, \rho_{\ell+1}$  // add/remove neurons

```

maximally representative (i.e., performance) and compact representations (e.g., width). Finally, the analysis of different functions f to soft-order neurons, for instance a power-law distribution or a sigmoid-like function, may have a different impact on convergence and performance and could be empirically investigated.

The current limitation of AWNN is the relative overhead to change the network at *training* time. A minimal and naïve implementation has up to 10x cost compared to a fixed network (this relative overhead may reduce for more compute-bound tasks). Besides optimizing our code, other optimizations are conceivable: i) by updating the width every M minibatches rather than at every step; ii) by allocating a larger network and dynamically grow it only if needed; iii) by creating ad-hoc support of AWNN on deep learning libraries like Pytorch. In any case, this overhead is relatively small compared to the exponential size of the hyper-parameter space when cross-validating the number of neurons of a multi-layered architecture.

4. Experiments and Setup

The purpose of the empirical analysis is **not** to claim AWNN is generally better than the fixed-width baseline. Rather, we demonstrate how AWNN overcomes the problem of fixing the number of neurons by learning it, thus reducing the amount of configurations to test. As such, due to the nature of this work and similarly to Mitchell et al. (2023), we use the remaining space to thoroughly study the behavior of AWNN, so that it becomes clear how to use it in practice. We first quantitatively verify that AWNN does not harm the performance compared to baseline models and compare the chosen width by means of grid-search model selection with the learned width of AWNN. Secondly, we check that AWNN chooses a higher width for harder tasks, which can be seen as increasing the hypotheses space until the neural network finds a good path to convergence. Third, we verify that convergence speed is not significantly altered by AWNN, so that the main limitation lies in the extra overhead for adapting the network at each training step. As a sanity

check, we study conditions under which AWNN’s learned width does not seem to depend on starting hyper-parameters, so that their choice does not matter much. Finally, we analyze other practical advantages of training a neural network under the AWNN framework: the ability to compress information during training or post training, and the resulting trade-offs. Further analyses are in the Appendix.

We now provide the details to reproduce our experiments on 9 datasets. We compare a baseline that undergoes proper hyper-parameter tuning against its AWNN version, where we replace any fixed MLP with an adaptive one. First, we train an MLP on 3 synthetic tabular tasks of increasing binary classification difficulty, namely a double moon, a spiral, and a double spiral that we call SpiralHard. A stratified hold-out split of 70% training/10% validation/20% test for risk assessment is chosen at random for these datasets. Similarly, we consider a ResNet-20 (He et al., 2016) trained on 3 image classification tasks, namely MNIST (LeCun, 1998), CIFAR10, and CIFAR100 (Krizhevsky, 2009), where data splits and preprocessing are taken from the original paper and AWNN is applied to the downstream classifier. In the graph domain, we train a Graph Isomorphism Network (Xu et al., 2019) on the NCI1 and REDDIT-B classification tasks using the same split and evaluation setup of Errica et al. (2020). These tasks are chosen as the structure was found to have a proper influence on the final performance. Here, the first 1 hidden layer MLP as well as the one used in each graph convolutional layer are replaced by adaptive AWNN versions. On all these tasks, the metric of interest is the accuracy. Finally, for the textual domain we train a Transformer architecture (Vaswani et al., 2017) on the Multi30k English-German translation task (Elliott et al., 2016), using a pretrained GPT-2 Tokenizer, and we evaluate the cross-entropy loss over the translated words. On tabular, image, and text-based tasks, an internal validation set (10%) for model selection is extracted from the union of outer training and validation sets, and the best configuration chosen according to the internal validation set is retrained 10 times on the outer train/validation/test splits, averaging test performances. Due to space reasons, we report datasets statistics and the hyper-parameter tried for the fixed and AWNN versions in Appendix B and C, respectively.

5. Results

We begin by discussing the quantitative results of our experiments: Table 1 reports means and standard deviations across the 10 final training runs. In terms of performance, we observe that AWNN is more stable or accurate than a fixed MLP on DoubleMoon, Spiral, and SpiralHard; all other things being equal, it seems that using more neurons and their soft ordering are the main contributing factors to these improvements. On the image datasets, performances

Table 1. We compare performances and total width of MLP layers for the fixed and AWNN versions of the various models used. The exact width chosen by model selection on the graph datasets is unknown since we report published results. ‘‘Linear’’ means that the chosen downstream classifier is a linear model.

	Fixed	AWNN		Width (Fixed)	Width (AWNN)	
	Mean	(Std)	Mean	(Std)	Mean	(Std)
DoubleMoon	100.0	(0.0)	100.0	(0.0)	8	8.1 (2.8)
Spiral	99.5	(0.5)	99.8	(0.1)	16	65.9 (8.7)
SpiralHard	98.0	(2.0)	100.0	(0.0)	32	227.4 (32.4)
MNIST	99.6	(0.1)	99.7	(0.0)	Linear	19.4 (4.8)
CIFAR10	91.4	(0.2)	91.4	(0.2)	Linear	80.1 (12.4)
CIFAR100	66.5	(0.4)	63.1	(4.0)	256	161.9 (57.8)
NCI1	80.0	(1.4)	80.0	(1.1)	(96-320)	731.3 (128.2)
REDDIT-B	87.0	(4.4)	90.2	(1.3)	(96-320)	793.6 (574.0)
Multi30k (↓)	1.43	(0.4)	1.51	(0.2)	24576	123.2 (187.9)

of AWNN are comparable to those of the fixed baseline but for CIFAR100, due to an unlucky run that did not converge. In this case, AWNN learns a smaller total width compared to grid search.

Results on graph datasets are interesting in two respects: First, the performance on REDDIT-B is significantly improved by AWNN both in terms of average performance and stability of results; second, the total learned width is significantly higher than those tried in Xu et al. (2019); Errica et al. (2020), meaning that a biased choice of a good range of width has had a profound influence on the estimation of the risk for a specific family of DGN models (i.e., GIN). This result makes it evident that it is important to let the network decide how many neurons are necessary to solve the task. To check that the learned width is indeed conducive to good performances, Appendix D shows what happens when we retrain some fixed baselines using the total width as the width of each layer.

Finally, the results on the Multi30k show that the AWNN Transformer learns to use 200x parameters less than the fixed Transformer for the feed-forward networks, achieving a statistically comparable test loss. This result is appealing when read through the lenses of modern deep learning, as the power required by some neural networks such as Large Language Models (Brown et al., 2020) is so high that cannot be afforded by most institutions, and it demands future investigations.

5.1. Adaptation to Task Difficulty and Convergence

Intuitively, one would expect that AWNN learned larger widths for more difficult tasks. This is indeed what happens on the tabular datasets (and image datasets, see Appendix E) where some tasks are clearly harder than others. Figure 3 (left) shows that, given the same starting width per layer, the learned number of neurons grows according to the task’s

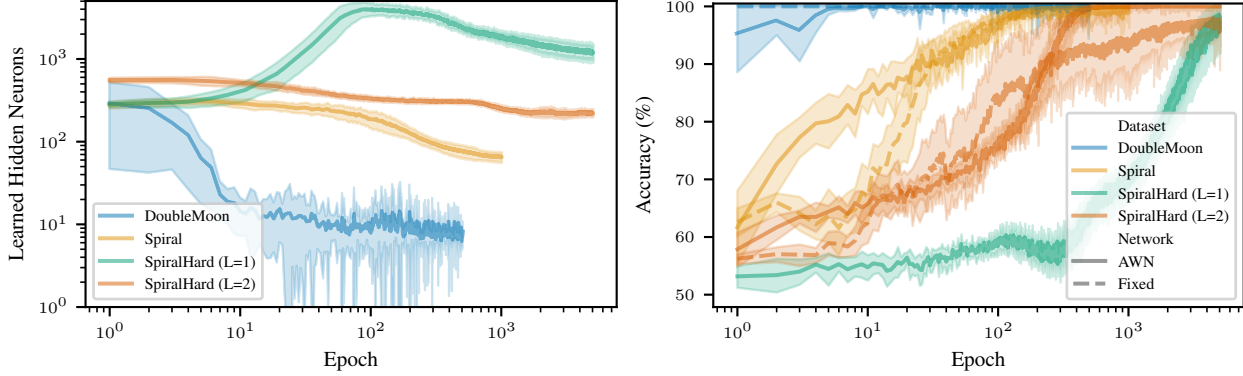


Figure 3. (Left) The learned width adapts to the increasing difficulty of the task, from the DoubleMoon to SpiralHard. (Right) AWNN reaches perfect test accuracy with a comparable amount of epochs on DoubleMoon and Spiral, while it converges faster on SpiralHard.

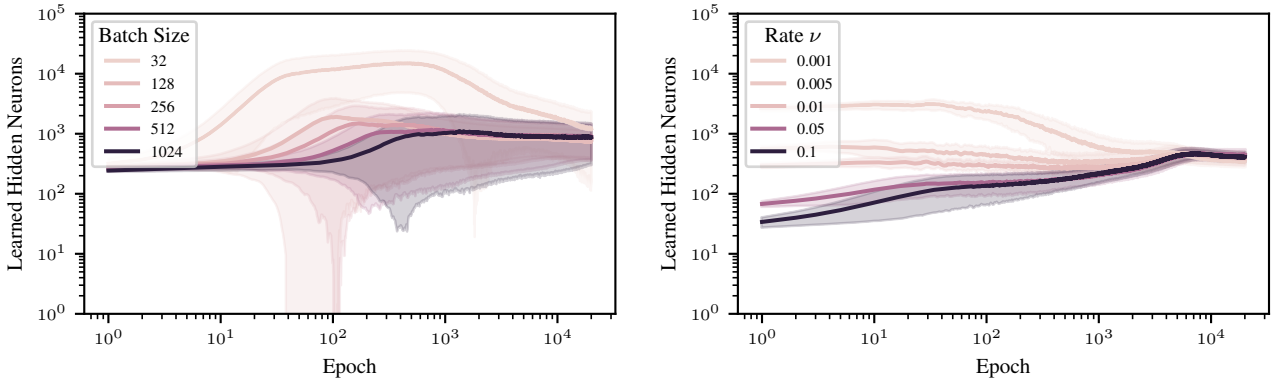


Figure 4. Training converges to similar widths on SpiralHard for different batch sizes (left) and starting rates ν , but the latter seems to require a bounded nonlinearity such as ReLU6 to converge in a reasonable amount of epochs (right).

difficulty. It is also interesting to observe that the total width for a multi-layer MLP on SpiralHard is significantly lower than that achieved by a single-layer MLP, which is consistent with the circuit complexity theory arguments put forward in Bengio et al. (2006). It also appears that convergence is not affected by the introduction of AWNN, as investigated in Figure 3 (right), which was not obvious considering the parametrization constraints encouraged by the rescaling of neurons’ activations.

5.2. Training Stability Analysis

To support our argument that AWNN can reduce the time spent performing hyper-parameter selection, it is instructive to check whether AWNN learns a consistent amount of neurons across different training runs and hyper-parameter choices. Figure 4 reports the impact of the batch size and starting width averaged across the different configurations tried during model selection. Smaller batch sizes cause more instability, but in the long run we observe convergence to a similar width. Convergence with respect to different

rates holds, instead, for the bounded ReLU6 activation; Appendix F shows that unbounded activations may cause the network to converge more slowly to the same width, which is in accord with the considerations about counterbalancing the rescaling effect of Section 3.1. Therefore, whenever possible, we recommend using bounded activations.

5.3. Online Network Compression via Regularization

So far, we have used an uninformative prior $p(\lambda)$ over the neural networks’ width. We demonstrate the effect of an informative prior by performing an annealing experiment on the SpiralHard dataset. We set an uninformative $p(\theta)$ and ReLU6 nonlinearity. At epoch 1000, we introduce $p(\lambda_\ell) = \mathcal{N}(\lambda_\ell; 0.05, 1)$, and gradually anneal the standard deviation up to 0.1 at epoch 2500. Figure 5 shows that the width of the network reduces from approximately 800 neurons to 300 without any test performance degradation. We hypothesize that the least important neurons mostly carry negligible information, and therefore they can be safely removed without drastic changes in the output of the model.

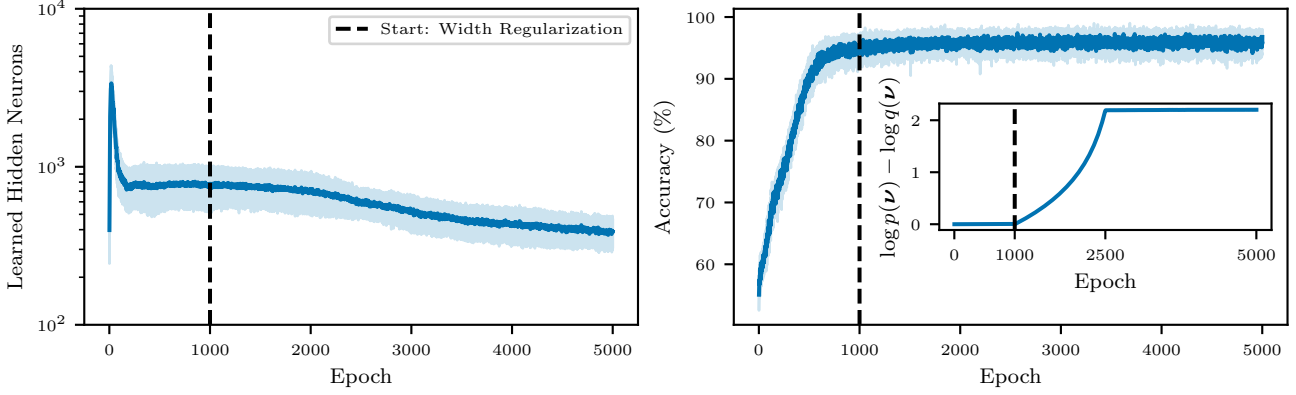


Figure 5. It is possible to regularize the width at training time by increasing the magnitude of the loss term $\log \frac{p(\nu)}{q(\nu)}$. The total width is reduced by more than 50% (left) while preserving accuracy (right). The inset plot refers to the loss term that AWNN tries to maximize.

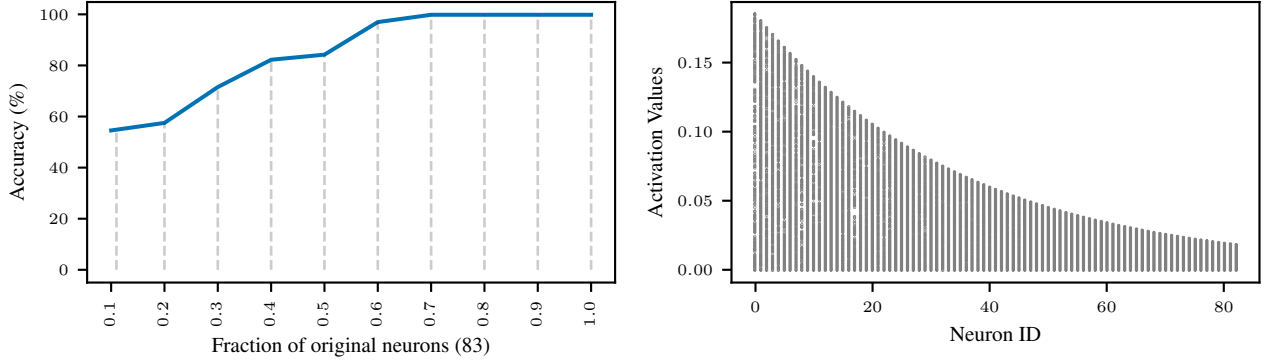


Figure 6. (Left) Thanks to the soft ordering imposed on the neurons, one can also truncate the neural network *after training* by simply removing the last neurons. (Right) The distribution of neurons' activations for all Spiral test samples follows an exponential-like curve.

This technique might be particularly useful to compress large models with billions of parameters.

5.4. Post-hoc Truncation achieves a trade-off between performance and compute resources

To further investigate the advantages of imposing a soft ordering of importance among neurons, we show that it is possible to perform hard network's truncation after training while still controlling the trade-off between performance and network size. Figure 6 shows an example for an MLP on the Spiral dataset, where the range of activation values (Equation 14) computed for all samples follows an exponential curve (right). Therefore, it is expected that removing the last neurons may have a negligible performance impact at the beginning and a drastic one as few neurons remain. This is what happens in the left plot, where we are able to cut an MLP with hidden width 83 by 30% without loss of accuracy, after which a smooth degradation happens. If one accepts such a trade-off, this technique may be used to distill a trained neural network at virtually zero additional cost while reducing the memory requirements.

6. Conclusions

We introduced a new methodology to learn an unbounded width of neural network layers within a single training, by imposing a soft ordering of importance among neurons. Our approach requires very few changes to the architecture, adapts the width to the task's difficulty, and does not impact negatively convergence, although it introduces some overhead during training. We showed stability convergence to similar widths under bounded activations for different hyper-parameters configurations, advocating for a practical reduction of the width's search space. A by-product of neurons' ordering is the ability to easily compress the network during or after training, which is relevant in the context of foundational models trained on large data, which are believed to require billions of parameters. Finally, we have tested AWNN on different models and data domains to prove its broad scope of applicability: a Transformer architecture achieved the same loss with **200x** less parameters.

Impact Statement

This paper presents work whose goal is to advance the field of Machine Learning. There are many potential societal consequences of our work, none of which we feel must be specifically highlighted here.

References

Barber, D. *Bayesian reasoning and machine learning*. Cambridge University Press, 2012.

Bender, G., Kindermans, P.-J., Zoph, B., Vasudevan, V., and Le, Q. Understanding and simplifying one-shot architecture search. In *Proceedings of the 35th International Conference on Machine Learning (ICML)*, 2018.

Bengio, Y., Lamblin, P., Popovici, D., and Larochelle, H. Greedy layer-wise training of deep networks. In *Proceedings of the 20th Conference on Neural Information Processing Systems (NIPS)*, 2006.

Bernardo, J. M. and Smith, A. F. *Bayesian theory*, volume 405. John Wiley & Sons, 2009.

Blalock, D., Gonzalez Ortiz, J. J., Frankle, J., and Guttag, J. What is the state of neural network pruning? In *Proceedings of machine learning and systems (MLSys)*, 2020.

Blei, D. M., Kucukelbir, A., and McAuliffe, J. D. Variational inference: A review for statisticians. *Journal of the American statistical Association*, 112(518):859–877, 2017.

Brock, A., Lim, T., Ritchie, J., and Weston, N. SMASH: One-shot model architecture search through hypernetworks. In *6th International Conference on Learning Representations (ICLR)*, 2018.

Brown, T. B., Mann, B., Ryder, N., Subbiah, M., Kaplan, J., Dhariwal, P., Neelakantan, A., Shyam, P., Sastry, G., Askell, A., Agarwal, S., Herbert-Voss, A., Krueger, G., Henighan, T., Child, R., Ramesh, A., Ziegler, D. M., Wu, J., Winter, C., Hesse, C., Chen, M., Sigler, E., Litwin, M., Gray, S., Chess, B., Clark, J., Berner, C., McCandlish, S., Radford, A., Sutskever, I., and Amodei, D. Language models are few-shot learners. *arXiv preprint*, abs/2005.14165, 2020.

Cybenko, G. Approximation by superpositions of a sigmoidal function. *Mathematics of control, signals and systems*, 2(4):303–314, 1989.

Domke, J. Generic methods for optimization-based modeling. In *Artificial Intelligence and Statistics*, pp. 318–326, 2012.

Dufort-Labbé, S., D’Oro, P., Nikishin, E., Pascanu, R., Bacon, P.-L., and Baratin, A. Maxwell’s demon at work: Efficient pruning by leveraging saturation of neurons. *arXiv preprint*, 2024.

Elliott, D., Frank, S., Sima’an, K., and Specia, L. Multi30k: Multilingual english-german image descriptions. In *Proceedings of the 5th Workshop on Vision and Language*, 2016.

Elsken, T., Metzen, J. H., and Hutter, F. Efficient multi-objective neural architecture search via lamarckian evolution. In *7th International Conference on Learning Representations (ICLR)*, 2019a.

Elsken, T., Metzen, J. H., and Hutter, F. Neural architecture search: A survey. *Journal of Machine Learning Research*, 20:1–21, 2019b.

Errica, F., Podda, M., Bacciu, D., and Micheli, A. A fair comparison of graph neural networks for graph classification. In *8th International Conference on Learning Representations (ICLR)*, 2020.

Fahlman, S. and Lebiere, C. The cascade-correlation learning architecture. In *Proceedings of the 3rd Conference on Neural Information Processing Systems (NIPS)*, 1989.

Franceschi, L., Donini, M., Frasconi, P., and Pontil, M. Forward and reverse gradient-based hyperparameter optimization. *ICML*, 2017.

Franceschi, L., Frasconi, P., Salzo, S., Grazzi, R., and Pontil, M. Bilevel programming for hyperparameter optimization and meta-learning. In *Proceedings of the 35th International Conference on Machine Learning (ICML)*, 2018.

Glorot, X. and Bengio, Y. Understanding the difficulty of training deep feedforward neural networks. In *Proceedings of the 13th International Conference on Artificial Intelligence and Statistics (AISTATS)*, 2010.

Goel, P. K. and Degroot, M. H. Information about hyperparamters in hierarchical models. *Journal of the American Statistical Association*, 76:140–147, 1981.

Gou, J., Yu, B., Maybank, S. J., and Tao, D. Knowledge distillation: A survey. *International Journal of Computer Vision*, 129(6):1789–1819, 2021.

He, K., Zhang, X., Ren, S., and Sun, J. Delving deep into rectifiers: Surpassing human-level performance on imagenet classification. In *Proceedings of the IEEE international Conference on Computer Vision (ICCV)*, pp. 1026–1034, 2015.

He, K., Zhang, X., Ren, S., and Sun, J. Deep residual learning for image recognition. In *Proceedings of the IEEE conference on Computer Vision and Pattern Recognition (CVPR)*, 2016.

Hinton, G., Vinyals, O., and Dean, J. Distilling the knowledge in a neural network. *arXiv preprint*, 2015.

Hochreiter, S. and Schmidhuber, J. Long short-term memory. *Neural Computation MIT-Press*, 1997.

Jordan, M. I., Ghahramani, Z., Jaakkola, T. S., and Saul, L. K. An introduction to variational methods for graphical models. *Machine learning*, 37:183–233, 1999.

Krizhevsky, A. Learning multiple layers of features from tiny images. *Master's thesis, University of Toronto*, 2009.

LeCun, Y. The mnist database of handwritten digits. <http://yann.lecun.com/exdb/mnist/>, 1998.

LeCun, Y., Boser, B., Denker, J. S., Henderson, D., Howard, R. E., Hubbard, W., and Jackel, L. D. Backpropagation applied to handwritten zip code recognition. *Neural computation*, 1(4):541–551, 1989.

LeCun, Y., Bengio, Y., and Hinton, G. Deep learning. *nature*, 521(7553):436–444, 2015.

Liu, H., Simonyan, K., and Yang, Y. DARTS: Differentiable architecture search. In *7th International Conference on Learning Representations (ICLR)*, 2019.

Maclaurin, D., Duvenaud, D., and Adams, R. Gradient-based hyperparameter optimization through reversible learning. In *International Conference on Machine Learning*, pp. 2113–2122, 2015.

Micheli, A. Neural network for graphs: A contextual constructive approach. *IEEE Transactions on Neural Networks*, 20(3):498–511, 2009.

Mishra, A., Latorre, J. A., Pool, J., Stosic, D., Stosic, D., Venkatesh, G., Yu, C., and Micikevicius, P. Accelerating sparse deep neural networks. *arXiv preprint*, 2021.

Mitchell, R., Mundt, M., and Kersting, K. Self expanding neural networks. *arXiv preprint*, 2023.

Mitchell, T. *Machine learning*. McGraw-hill, 1997.

Nazaret, A. and Blei, D. Variational inference for infinitely deep neural networks. In *Proceedings of the 39th International Conference on Machine Learning (ICML)*, 2022.

Orbanz, P. and Teh, Y. W. Bayesian nonparametric models. *Encyclopedia of machine learning*, 1, 2010.

Paszke, A., Gross, S., Chintala, S., Chanan, G., Yang, E., DeVito, Z., Lin, Z., Desmaison, A., Antiga, L., and Lerer, A. Automatic differentiation in pytorch. In *Proceedings of the 31st Conference on Neural Information Processing Systems (NIPS)*, 2017.

Pham, H., Guan, M., Zoph, B., Le, Q., and Dean, J. Efficient neural architecture search via parameters sharing. In *Proceedings of the 35th International Conference on Machine Learning (ICML)*, 2018.

Prechelt, L. Early stopping-but when? In *Neural Networks: Tricks of the trade*, pp. 55–69. Springer, 1998.

Real, E., Aggarwal, A., Huang, Y., and Le, Q. V. Regularized evolution for image classifier architecture search. In *Proceedings of the 33rd AAAI Conference on Artificial Intelligence (AAAI)*, 2019.

Rosenblatt, F. The perceptron: a probabilistic model for information storage and organization in the brain. *Psychological review*, 65(6):386, 1958.

Roy, D. The discrete normal distribution. *Communications in Statistics - Theory and Methods*, 32:1871–1883, 2003. doi: 10.1081/sta-120023256.

Rumelhart, D. E., Hinton, G. E., and Williams, R. J. Learning representations by back-propagating errors. *Nature*, 323:533–536, 1986.

Scarselli, F., Gori, M., Tsoi, A. C., Hagenbuchner, M., and Monfardini, G. The graph neural network model. *IEEE Transactions on Neural Networks*, 20(1):61–80, 2009.

So, D. R., Liang, C., and Le, Q. V. The evolved transformer. In *Proceedings of the 36th International Conference on Machine Learning (ICML)*, 2019.

Tishby, N., Pereira, F. C., and Bialek, W. The information bottleneck method. *arXiv preprint*, 2000.

Valerio, L., Nardini, F. M., Passarella, A., and Perego, R. Dynamic hard pruning of neural networks at the edge of the internet. *Journal of Network and Computer Applications*, 200:103330, 2022.

Vaswani, A., Shazeer, N., Parmar, N., Uszkoreit, J., Jones, L., Gomez, A. N., Kaiser, L., and Polosukhin, I. Attention is all you need. In *Proceedings of the 31st Conference on Neural Information Processing Systems (NIPS)*, 2017.

White, C., Nolen, S., and Savani, Y. Local search is state of the art for nas benchmarks. In *Proceedings of the 37th Uncertainty in Artificial Intelligence Conference (UAI)*, 2021.

White, C., Safari, M., Sukthanker, R., Ru, B., Elsken, T., Zela, A., Dey, D., and Hutter, F. Neural architecture search: Insights from 1000 papers. *arXiv preprint*, 2023.

Wolpert, D. H. The lack of a priori distinctions between learning algorithms. *Neural computation*, 8(7):1341–1390, 1996.

Wu, L., Wang, D., and Liu, Q. Splitting steepest descent for growing neural architectures. In *Proceedings of the 33rd Conference on Neural Information Processing Systems (NeurIPS)*, 2019.

Wu, L., Liu, B., Stone, P., and Liu, Q. Firefly neural architecture descent: a general approach for growing neural networks. In *Proceedings of the 34th Conference on Neural Information Processing Systems (NeurIPS)*, volume 33, 2020.

Xu, K., Hu, W., Leskovec, J., and Jegelka, S. How powerful are graph neural networks? In *7th International Conference on Learning Representations (ICLR)*, 2019.

Yoon, J., Yang, E., Lee, J., and Hwang, S. J. Lifelong learning with dynamically expandable networks. In *6th International Conference on Learning Representations (ICLR)*, 2018.

Zhai, X., Kolesnikov, A., Houlsby, N., and Beyer, L. Scaling vision transformers. In *Proceedings of the IEEE/CVF conference on Computer Vision and Pattern Recognition (CVPR)*, 2022.

Zhang, L., Song, J., Gao, A., Chen, J., Bao, C., and Ma, K. Be your own teacher: Improve the performance of convolutional neural networks via self distillation. In *Proceedings of the IEEE/CVF International Conference on Computer Vision (ICCV)*, 2019.

Zoph, B. and Le, Q. V. Neural architecture search with reinforcement learning. In *4th International Conference on Learning Representations (ICLR)*, 2016.

Zoph, B., Vasudevan, V., Shlens, J., and Le, Q. V. Learning transferable architectures for scalable image recognition. *Proceedings of the IEEE conference on Computer Vision and Pattern Recognition (CVPR)*, 2018.

A. Full derivation of the rescaled weight initialization

This Section derives the formulas for the rescaled weight initialization both in the case of ReLU and activations like tanh.

Background We can rewrite Equation 14 as

$$h_i^\ell = \alpha_i^\ell p_i^\ell \quad (16)$$

$$\alpha_i^\ell = \sigma \left(\sum_{j=1}^{D_{\ell-1}} w_{ij}^\ell \underbrace{\alpha_j^{\ell-1} p_j^{\ell-1}}_{h_j^{\ell-1}} \right) \quad (17)$$

where $p_i^\ell = f_\ell(i)$.

As a refresher, the chain rule of calculus states that, given two differentiable functions $g : \mathbb{R}^D \rightarrow \mathbb{R}$ and $f = (f_1, \dots, f_D) : \mathbb{R} \rightarrow \mathbb{R}^D$, their composition $g \circ f : \mathbb{R} \rightarrow \mathbb{R}$ is differentiable and

$$\begin{aligned} (g \circ f)'(t) &= \nabla g(f(t))^T f'(t) \\ \nabla g(f(t)) &= \left(\frac{\partial g(f_1(t))}{\partial f_1(t)}, \dots, \frac{\partial g(f_D(t))}{\partial f_D(t)} \right) \in \mathbb{R}^{1 \times D} \\ f'(t) &= (f'_1(t), \dots, f'_D(t)) \in \mathbb{R}^{D \times 1} \end{aligned}$$

For reasons that will become clear later, we may want to compute the gradient of the loss function with respect to the intermediate activations α^ℓ at a given layer, that is $\nabla \mathcal{L}(\alpha^\ell) = \left(\frac{\partial \mathcal{L}(\alpha_1^\ell)}{\partial \alpha_1^\ell}, \dots, \frac{\partial \mathcal{L}(\alpha_{N^\ell}^\ell)}{\partial \alpha_{N^\ell}^\ell} \right)$. We focus on the i -th partial derivative $\frac{\partial \mathcal{L}(\alpha_i^\ell)}{\partial \alpha_i^\ell}$, where the only variable is α_i^ℓ . Then, we view the computation of the loss function starting from α_i^ℓ as a composition of a function $\alpha^{\ell+1} : \mathbb{R} \rightarrow \mathbb{R}^{N^{\ell+1}} = (\alpha_1^{\ell+1}(\alpha_i^\ell), \dots, \alpha_{N^{\ell+1}}^{\ell+1}(\alpha_i^\ell))$ and another function (abusing the notation) $\mathcal{L} : \mathbb{R}^{N^{\ell+1}} \rightarrow \mathbb{R}$ that computes the loss value starting from $\alpha^{\ell+1}$. By the chain rule:

$$\frac{\partial \mathcal{L}(\alpha_i^\ell)}{\partial \alpha_i^\ell} = \underbrace{\left(\frac{\partial \mathcal{L}(\alpha_1^{\ell+1})}{\partial \alpha_1^{\ell+1}}, \dots, \frac{\partial \mathcal{L}(\alpha_{N^{\ell+1}}^{\ell+1})}{\partial \alpha_{N^{\ell+1}}^{\ell+1}} \right)^T}_{\nabla g(f(t))^T} \underbrace{\left(\frac{\partial \alpha_1^{\ell+1}(\alpha_i^\ell)}{\partial \alpha_i^\ell}, \dots, \frac{\partial \alpha_{N^{\ell+1}}^{\ell+1}(\alpha_i^\ell)}{\partial \alpha_i^\ell} \right)}_{f'(t)} \quad (18)$$

Theorem 3.1 Let us consider an MLP with activations as in Equation 17. Let us also assume that the inputs and the parameters have been sampled independently from a Gaussian distribution with zero mean and variance $\sigma^2 = \text{Var}[w_{ij}^\ell] \forall i, j, \ell$. At initialization, the variance of the responses α_i^ℓ across layers is constant if, $\forall \ell \in \{1, \dots, L\}$

$$\text{Var}[w^\ell] = \frac{1}{\sum_j^{D_{\ell-1}} (p_j^{\ell+1})^2} \text{ for activation } \sigma \text{ such that } \sigma'(0) \approx 1 \quad (19)$$

$$\text{Var}[w^\ell] = \frac{2}{\sum_j^{D_{\ell-1}} (p_j^{\ell+1})^2} \text{ for the ReLU activation.} \quad (20)$$

In addition, we provide closed form formulas to preserve the variance of the gradient across layers.

Proof. Let us start from the first case of $\sigma'(0) \approx 1$. Using the Taylor expansions for the moments of functions of random variables as in Glorot & Bengio (2010)

$$\text{Var}[\alpha_i^\ell] = \text{Var} \left[\sigma \left(\sum_{j=1}^{D_{\ell-1}} w_{ij}^\ell \alpha_j^{\ell-1} p_j^{\ell-1} \right) \right] \quad (21)$$

$$\approx \sigma' \left(\mathbb{E} \left[\sum_{j=1}^{D_{\ell-1}} w_{ij}^\ell \alpha_j^{\ell-1} p_j^{\ell-1} \right] \right) \text{Var} \left[\sum_{j=1}^{D_{\ell-1}} w_{ij}^\ell \alpha_j^{\ell-1} p_j^{\ell-1} \right] \quad (22)$$

Using the fact that p_j is a constant and that w and α are independent from each other

$$\mathbb{E} \left[\sum_{j=1}^{D_{\ell-1}} w_{ij}^\ell \alpha_j^{\ell-1} p_j^{\ell-1} \right] = \sum_{j=1}^{D_{\ell-1}} \underbrace{\mathbb{E}[w_{ij}^\ell]}_0 \mathbb{E}[\alpha_j^{\ell-1}] p_j^{\ell-1} = 0. \quad (23)$$

Therefore, recalling that $\sigma'(0) \approx 1$

$$\sigma' \left(\mathbb{E} \left[\sum_{j=1}^{D_{\ell-1}} w_{ij}^\ell \alpha_j^{\ell-1} p_j^{\ell-1} \right] \right) = 1. \quad (24)$$

As a result, we arrive at

$$\text{Var}[\alpha_i^\ell] \approx \text{Var} \left[\sum_{j=1}^{D_{\ell-1}} w_{ij}^\ell \alpha_j^{\ell-1} p_j^{\ell-1} \right]. \quad (25)$$

Because w and α are independent, they are also uncorrelated and their variances sum. Also, using the fact that $\text{Var}[aX] = a^2 \text{Var}[X]$ for a constant a ,

$$\text{Var} \left[\sum_{j=1}^{D_{\ell-1}} w_{ij}^\ell \alpha_j^{\ell-1} p_j^{\ell-1} \right] = \sum_{j=1}^{D_{\ell-1}} \text{Var} [w_{ij}^\ell \alpha_j^{\ell-1} p_j^{\ell-1}] = \sum_{j=1}^{D_{\ell-1}} \text{Var} [w_{ij}^\ell \alpha_j^{\ell-1}] (p_j^{\ell-1})^2 \quad (26)$$

Finally, because the mean of the independent variables involved is zero by assumption, it holds that $\text{Var}[w_{ij}^\ell \alpha_j^{\ell-1}] = \text{Var}[w_{ij}^\ell] \text{Var}[\alpha_j^{\ell-1}]$. We can also abstract from the indexes, since the weight variables are i.i.d. and from that it follows that $\text{Var}[\alpha_i^\ell] = \text{Var}[\alpha_j^\ell] \forall i, j, i, j \in \{1, \dots, D_\ell\}$, obtaining³

$$\text{Var}[\alpha^\ell] \approx \text{Var}[w^\ell] \text{Var}[\alpha^{\ell-1}] \sum_{j=1}^{D_{\ell-1}} (p_j^{\ell-1})^2, \quad (27)$$

noting again that the previous equation does not depend on i . We want to impose $\text{Var}[\alpha^\ell] \approx \text{Var}[\alpha^{\ell-1}]$, which can be achieved whenever

$$\text{Var}[w^\ell] \approx \frac{1}{\sum_{j=1}^{D_{\ell-1}} (p_j^{\ell-1})^2}. \quad (28)$$

Condition on the gradients From a backpropagation perspective, a similar desideratum would be to ensure that $\text{Var} \left[\frac{\partial \mathcal{L}(\alpha_i^\ell)}{\partial \alpha_i^\ell} \right] = \text{Var} \left[\frac{\partial \mathcal{L}(\alpha_j^{\ell+1})}{\partial \alpha_j^{\ell+1}} \right]$ ⁴.

Using Equation 18, and considering as in Glorot & Bengio (2010) that at initialization we are in a linear regime where $\sigma'(x) \approx 1$,

$$\text{Var} \left[\frac{\partial \mathcal{L}(\alpha_i^\ell)}{\partial \alpha_i^\ell} \right] = \text{Var} \left[\sum_{j=1}^{D_{\ell+1}} \frac{\partial \mathcal{L}(\alpha_j^{\ell+1})}{\partial \alpha_j^{\ell+1}} \frac{\partial \alpha_j^{\ell+1}(\alpha_i^\ell)}{\partial \alpha_i^\ell} \right] = \text{Var} \left[\sum_{j=1}^{D_{\ell+1}} \frac{\partial \mathcal{L}(\alpha_j^{\ell+1})}{\partial \alpha_j^{\ell+1}} \frac{\partial \alpha_j^{\ell+1}(\alpha_i^\ell)}{\partial \alpha_i^\ell} \right] \quad (29)$$

$$= \text{Var} \left[\sum_{j=1}^{D_{\ell+1}} \frac{\partial \mathcal{L}(\alpha_j^{\ell+1})}{\partial \alpha_j^{\ell+1}} \underbrace{\sigma' \left(\sum_{k=1}^{D_\ell} w_{jk}^{\ell+1} \alpha_k^\ell p_k^\ell \right)}_{\approx 1} w_{ji}^{\ell+1} p_i^\ell \right]. \quad (30)$$

³It is worth noting that, in standard MLPs, $p_j^\ell = 1$ so we recover the derivation of Glorot & Bengio (2010), since $\sum_{j=1}^{D_{\ell-1}} (p_j^{\ell-1})^2$ would be equal to $D_{\ell-1}$. In Glorot & Bengio (2010) our $D_{\ell-1}$ is denoted as “ $n_{i'}$ ” (see Equation 5).

⁴Note that what we impose is different from Glorot & Bengio (2010), where the specific position i is irrelevant. Here, we are asking that the variance of the gradients for neurons in the same position i , but at different layers, stays constant. Alternatively, we could impose an equivalence for all $i \neq i'$.

Using the same arguments as above one can write

$$\text{Var} \left[\frac{\partial \mathcal{L}(\alpha_i^\ell)}{\partial \alpha_i^\ell} \right] \approx \text{Var}[w^{\ell+1}] \sum_{j=1}^{D_{\ell+1}} \text{Var} \left[\frac{\partial \mathcal{L}(\alpha_j^{\ell+1})}{\partial \alpha_j^{\ell+1}} p_i^\ell \right] = \text{Var}[w^{\ell+1}] (p_i^\ell)^2 \sum_{j=1}^{D_{\ell+1}} \text{Var} \left[\frac{\partial \mathcal{L}(\alpha_j^{\ell+1})}{\partial \alpha_j^{\ell+1}} \right]. \quad (31)$$

Expanding, we get

$$\text{Var}[w^{\ell+1}] (p_i^\ell)^2 \sum_{j=1}^{D_{\ell+1}} \text{Var} \left[\frac{\partial \mathcal{L}(\alpha_j^{\ell+1})}{\partial \alpha_j^{\ell+1}} \right] = (p_i^\ell)^2 \left(\prod_{i=\ell+1}^{\ell+2} \text{Var}[w^{\ell+1}] \right) \sum_{j=1}^{D_{\ell+1}} (p_j^{\ell+1})^2 \underbrace{\left(\sum_{j'=1}^{D_{\ell+2}} \text{Var} \left[\frac{\partial \mathcal{L}(\alpha_{j'}^{\ell+2})}{\partial \alpha_{j'}^{\ell+2}} \right] \right)}_{\text{constant w.r.t. } j} \quad (32)$$

$$= (p_i^\ell)^2 \left(\prod_{i=\ell+1}^{\ell+2} \text{Var}[w^{\ell+1}] \right) \left(\sum_{j'=1}^{D_{\ell+2}} \text{Var} \left[\frac{\partial \mathcal{L}(\alpha_{j'}^{\ell+2})}{\partial \alpha_{j'}^{\ell+2}} \right] \right) \left(\sum_{j=1}^{D_{\ell+1}} (p_j^{\ell+1})^2 \right) \quad (33)$$

Therefore, we can recursively expand these terms and obtain

$$\text{Var} \left[\frac{\partial \mathcal{L}(\alpha_i^\ell)}{\partial \alpha_i^\ell} \right] = (p_i^\ell)^2 \left(\prod_{k=\ell+1}^L \text{Var}[w^k] \right) \left(\sum_{j'=1}^{D_L} \text{Var} \left[\frac{\partial \mathcal{L}(\alpha_{j'}^{D_L})}{\partial \alpha_{j'}^{D_L}} \right] \right) \left(\prod_{k=\ell+1}^{L-1} \sum_{j_k=1}^{D_k} (p_{j_k}^k)^2 \right). \quad (34)$$

In this case, the variance depends on i just for the term $(p_i^\ell)^2$. Finally, by imposing

$$\text{Var} \left[\frac{\partial \mathcal{L}(\alpha_i^\ell)}{\partial \alpha_i^\ell} \right] = \text{Var} \left[\frac{\partial \mathcal{L}(\alpha_i^{\ell+1})}{\partial \alpha_i^{\ell+1}} \right] \quad (35)$$

and simplifying common terms we obtain

$$(p_i^\ell)^2 \text{Var}[w^{\ell+1}] \left(\sum_{j=1}^{D_{\ell+1}} (p_j^{\ell+1})^2 \right) = (p_i^{\ell+1})^2 \quad (36)$$

$$\text{Var}[w^{\ell+1}] = \frac{(p_i^{\ell+1})^2}{(p_i^\ell)^2 \sum_{j=1}^{D_{\ell+1}} (p_j^{\ell+1})^2}. \quad (37)$$

Both Equations 28 and 37 are verified when we initialize the distributions f_ℓ in the same way for all layers, which implies $(p_i^\ell)^2 = (p_i^{\ell+1})^2$. Note that without this last requirement, Equation 37 would violate the i.i.d. assumption of the weights.

To show a similar initialization for ReLU activations, we need the following lemma.

Lemma A.1. *Consider the ReLU activation $y = \max(0, x)$ and a symmetric distribution $p(x)$ around zero. Then $\mathbb{E}[y^2] = \frac{1}{2} \text{Var}[x]$.*

Proof.

$$\mathbb{E}[y^2] = \int_{-\infty}^{+\infty} \max(0, x)^2 p(x) dx = \int_0^{+\infty} x^2 p(x) dx = \frac{1}{2} \int_{-\infty}^{+\infty} x^2 p(x) dx \quad (38)$$

Because $p(x)$ is symmetric, $\mathbb{E}[x] = 0$. Then

$$\frac{1}{2} \int_{-\infty}^{+\infty} x^2 p(x) dx = \frac{1}{2} \int_{-\infty}^{+\infty} (x - \mathbb{E}[x])^2 p(x) dx = \frac{1}{2} \text{Var}[x]. \quad (39)$$

□

Using Lemma A.1, we can rewrite Equation 22 as

$$\text{Var}[\alpha_i^\ell] = \text{Var} \left[\sigma \left(\sum_{j=1}^{D_{\ell-1}} w_{ij}^\ell \alpha_j^{\ell-1} p_j^{\ell-1} \right) \right] = \frac{1}{2} \text{Var} \left[\sum_{j=1}^{D_{\ell-1}} w_{ij}^\ell \alpha_j^{\ell-1} p_j^{\ell-1} \right] = \frac{1}{2} \text{Var}[w^\ell] \text{Var}[\alpha^{\ell-1}] \sum_{j=1}^{D_{\ell-1}} (p_j^{\ell-1})^2 \quad (40)$$

where no approximation has been made. Similar to prior results, it follows that

$$\text{Var}[w^\ell] = \frac{2}{\sum_{j=1}^{D_{\ell-1}} (p_j^{\ell-1})^2}. \quad (41)$$

From a backpropagation perspective, since $\sigma'(x) \approx 1$, we use similar arguments as in He et al. (2015): we assume that the pre-activations α have zero mean, then the derivative of the ReLU can have values zero or one with equal probability. One can show, by expanding the definition of variance, that $\text{Var}[\sigma' \left(\sum_{k=1}^{D_\ell} w_{jk}^{\ell+1} \alpha_k^\ell p_k^\ell \right) w_{ji}^{\ell+1}] = \frac{1}{2} \text{Var}[w_{ji}^{\ell+1}]$. As a result, one can re-write Equation 22 as

$$\text{Var} \left[\sum_{j=1}^{D_{\ell+1}} \frac{\partial \mathcal{L}(\alpha_j^{\ell+1})}{\partial \alpha_j^{\ell+1}} \sigma' \left(\sum_{k=1}^{D_\ell} w_{jk}^{\ell+1} \alpha_k^\ell p_k^\ell \right) w_{ji}^{\ell+1} p_i^\ell \right] \quad (42)$$

$$\approx \frac{1}{2} \text{Var}[w^{\ell+1}] (p_i^\ell)^2 \sum_{j=1}^{D_{\ell+1}} \text{Var} \left[\frac{\partial \mathcal{L}(\alpha_j^{\ell+1})}{\partial \alpha_j^{\ell+1}} \right], \quad (43)$$

where we have made a rough assumption of independence between $\sigma' \left(\sum_{k=1}^{D_\ell} w_{jk}^{\ell+1} \alpha_k^\ell p_k^\ell \right)$ and $w_{ji}^{\ell+1}$ since the former term is likely a constant. Following an identical derivation as above, we obtain

$$\text{Var}[w^{\ell+1}] = \frac{2(p_i^{\ell+1})^2}{(p_i^\ell)^2 \sum_{j=1}^{D_{\ell+1}} (p_j^{\ell+1})^2} \quad (44)$$

which is almost identical to Equation 41 and not dependent on i when we initialize f_ℓ in the same way for all layers. \square

Comparison of convergence for different initializations Below, we provide a comparison of convergence between an AWNN ReLU MLP initialized with the standard kaiming scheme and one initialized according to our theoretical results (“kaiming+”).

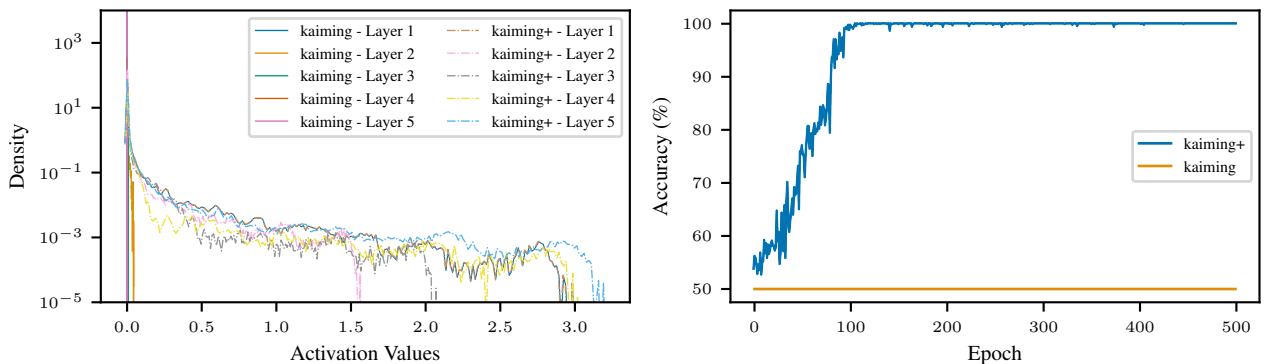


Figure 7. (Left) Effect of the rescaled initialization scheme (“kaiming+”) on a ReLU-based MLP, where neurons’ activations are computed using Equation 14. Compared to the standard initialization, the variance of activations agrees with the theoretical result. (Right) Without the rescaled initialization, convergence is hard to attain on the SpiralHard dataset (please refer to the next section for details about the dataset).

B. Dataset Info and Statistics

The synthetic datasets DoubleMoon, Spiral, and SpiralHard are shown in Figure 8. These binary classification datasets have been specifically created to analyze the behavior of AWNN in a controlled scenario where we are sure that the difficulty of the task increases. We provide the code to generate these datasets in the supplementary material.

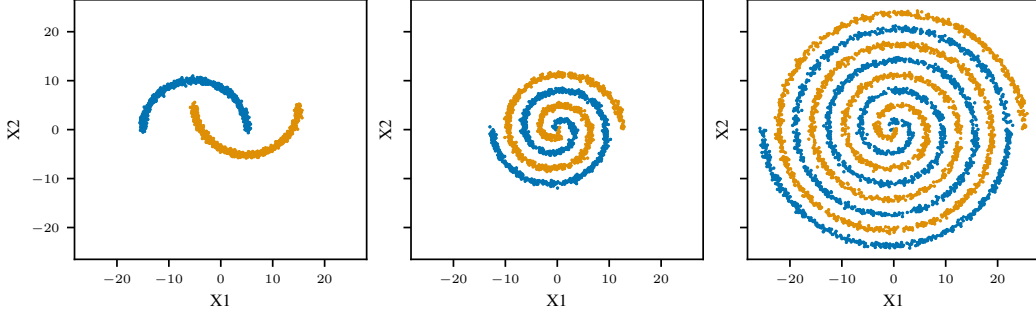


Figure 8. The DoubleMoon, Spiral, and SpiralHard synthetic datasets are used to test AWNN’s inner workings, and are ordered difficulty. Orange and blue colors denote different classes.

Table 2 reports information on their base statistics and the data splits created to carry out model selection (inner split) and risk assessment (outer split), respectively. Note that for Multi30k, the maximum sequence length is 128 and the number of

Table 2. Dataset statistics and number of samples in each split are shown.

	# Samples	# Features	# Classes	Outer Split (TR/VL/TE)	Inner Split (TR/VL)
DoubleMoon	2500	2	2	1750/250/500	1800/200
Spiral	2500	2	2	1750/250/500	1800/200
SpiralHard	5000	2	2	3500/500/1000	3600/400
MNIST	70000	28x28	10	53000/7000/10000	54000/6000
CIFAR10	60000	32x32x3	10	44000/6000/10000	45000/5000
CIFAR100	60000	32x32x3	100	44000/6000/10000	45000/5000
NCI1	4110	37	2	3288/411/411	3329/370
REDDIT-B	2000	1	2	1800/100/100	1710/190
Multi30k	31000	128x50257	Multilabel	29000/1000/1000	29000/1000

possible tokens is 50527. The classification loss is computed by comparing the predicted token against the expected one, ignoring any token beyond the length of the actual target. For a detailed description of the graph datasets, the reader can refer to Errica et al. (2020).

C. Hyper-parameters for fixed and AWNN models

For each data domain, we discuss the set of hyper-parameters tried during model selection for the fixed baseline and for AWNN. We try our best to keep architectural choices identical with the exception of the width of the MLPs used by each model. In all experiments, we either run patience-based early stopping (Prechelt, 1998) or simply select the epoch with best validation score.

C.1. Synthetic Tabular Datasets

We report the hyper-parameter configurations tried for the fixed MLP and AWNN in Table 3. In particular, the starting width of AWNN under the quantile function evaluated at $k = 0.9$ is approximately 256 hidden neurons. We also noticed that a learning rate value of 0.1 makes learning the width unstable, so we did not use it in our experiments. The total number of configurations for the fixed MLP is 180, for AWNN is 18. We also did not impose any prior on an expected size to see if AWNN recovers a similar width compared to the best fixed model (please refer to Table 1) starting from the largest configuration among the fixed models.

Table 3. Hyper-parameter configurations for standard MLP and AWNN versions on tabular datasets.

Hyper-Parameter	DoubleMoon	Spiral	SpiralHard
Batch Size	32	[32, 128] (MLP), 128 (AWNN)	[32, 128] (MLP), 128 (AWNN)
Epochs	500	1000	5000
Hidden Layers	1	1	[1, 2, 4]
Layer Width		[8, 16, 24, 128, 256]	
Non-linearity		[ReLU, LeakyReLU, ReLU6]	
Optimizer		Adam, learning rate $\in [0.1, 0.01]$ (MLP), 0.01 (AWNN)	
AWNN Specific			
Quantile Fun. Threshold k		0.9	
Exponential Distributions Rate		0.01	
σ_ℓ^θ		[1.0, 10.0]	
Prior over λ		Uninformative	

C.2. Image Classification Datasets

We train from scratch a ResNet20 and focus our architectural choices on the MLP that performs classification using the flattened representation provided by the previous CNN layers. This ensures that any change in performance is only due to the changes we apply to the MLP. The configurations are shown in Table 4; note that a width of 0 implies a linear classifier instead of a 1 hidden layer MLP. After previous results on tabular datasets showed that a LeakyReLU performs very well, we fixed it in the rest of the experiments. In this case, we test 5 different configurations of the fixed baseline, whereas we do

Table 4. Hyper-parameter configurations for standard MLP and AWNN versions on image classification datasets.

Hyper-Parameter	MNIST / CIFAR10 / CIFAR100
Batch Size	128
Epochs	200
Layer Width (classification layer)	[0, 32, 128, 256, 512]
Optimizer	SGD, learning rate 0.1, weight decay 0.0001, momentum 0.9
Scheduler	Multiply learning rate by 0.1 at epochs 50, 100, 150
AWNN Specific	
Quantile Fun. Threshold k	0.9
Exponential Distributions Rate	0.02
σ_ℓ^θ	1.0
Prior over λ	Uninformative

not have to perform any model selection for AWNN. The rate of the exponential distribution has been chosen to have a starting width of approximately 128 neurons, which is the median value among the ones tried for the fixed model.

C.3. Text Translation Tasks

Due to the cost of training a Transformer architecture from scratch on a medium size dataset like Multi30k, we use most hyper-parameters’ configurations of the base Transformer in [Vaswani et al. \(2017\)](#), with the difference that AWNN is applied to the MLPs in each encoder and decoder layer. We train an architecture with 6 encoder and 6 decoder layers for 500 epochs, with a patience of 250 epochs applied to the validation loss. We use an Adam optimizer with learning rate 0.01, weight decay 5e-4, and epsilon 5e-9. We also introduce a scheduler that reduces the learning rate by a factor 0.9 when a plateau in the loss is reached. The number of attention heads is set to 8 and the dropout to 0.1. We try different widths for the MLPs, namely [128,256,512,1024,2048]. The embedding size is fixed to 512 and the batch size is 128. The AWNN version starts with an exponential distribution rate of 0.004, corresponding to approximately 512 neurons, and a $\sigma_\ell^\alpha=1$.

C.4. Graph Classification Tasks

We train the AWNN version of Graph Isomorphism Network, following the setup of [Errica et al. \(2020\)](#) and reusing the published results. We test 12 configurations as shown in the table below. Please note that an extra MLP with 1 hidden layer is always placed before the sequence of graph convolutional layers.

Table 5. Hyper-parameter configurations for AWNN versions on graph classification datasets.

Hyper-Parameter	NCI1 / REDDIT-B
Batch Size	[32,128]
Epochs	1000
Graph Conv. Layers	[1, 2, 4]
Global Pooling	[sum, mean]
Optimizer	Adam, learning rate 0.01
AWNN Specific	
Patience	500 epochs
Quantile Fun. Threshold k	0.9
Exponential Distributions Rate	0.02
σ_ℓ^θ	10.0
Prior over λ	Uninformative

D. Re-training a fixed network with the learned width

While on DoubleMoon AWNN learns a similar number of neurons chosen by the model selection procedure and the convergence to the perfect solution over 10 runs seem much more stable, this is not the case on Spiral, SpiralHard and REDDIT-B, where AWNN learns a higher total width over layers. To investigate whether the width learned by AWNN on these datasets is indeed the reason behind the better performances (either a more stable training or better accuracy), we run again the experiments on the baseline networks, this time by fixing the width of each layer to the average width over hidden layers learned by AWNN and reported in Table 1. We call this experiment “Fixed+”.

	Spiral	SpiralHard	REDDIT-B
Fixed	99.5(0.5)	98.0(2.0)	87.0(4.4)
AWNN	99.8(0.1)	100.0(0.0)	90.2(1.3)
Fixed+	100.0(0.1)	83.2(17.0)	90.7(1.4)

The results suggest that by using more neurons than those selected by grid search – possibly because the validation results were identical between different configurations – it is actually possible to improve both accuracy and stability of results on Spiral and REDDIT-B, while we had a convergence issue on SpiralHard. Notice that the number of neurons learned by AWNN on REDDIT-B was well outside of the range investigated by [Xu et al. \(2019\)](#) and [Errica et al. \(2020\)](#), demonstrating that the practitioner’s bias can play an important role on the final performance.

E. Further qualitative results on image classification datasets

Because it is well known that MNIST, CIFAR10, and CIFAR100 are datasets of increasing difficulty, we attach a figure depicting the learned number of neurons and the convergence of AWNN on these datasets, following the practices highlighted in He et al. (2016) and described in Table 4 to bring the ResNet20 to convergence. Akin to the tabular datasets, we see a clear pattern where the learned number of neurons, averaged over the 10 final training runs, increases together with the task difficulty. The AWNN version of the ResNet20 converges in the same amount of epochs as the fixed one.

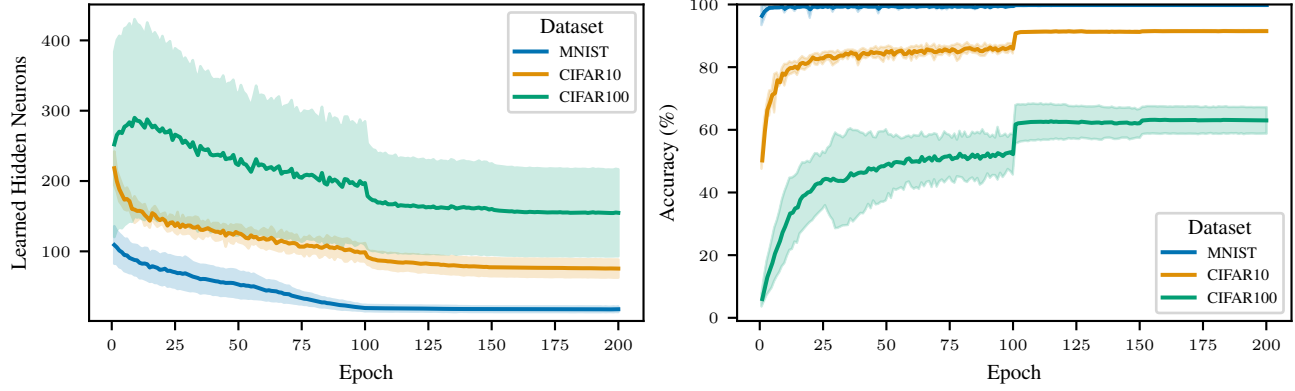


Figure 9. We present an analysis similar to Figure 3 but for image classification datasets of increasing difficulty. One can observe the jumps caused by the learning rate's scheduling strategy.

F. Non-linearity ablation study

Below, we report an ablation study on the impact of non-linear activation functions. We analyze the convergence to the same width across different batch sizes and exponential starting rates λ on the SpiralHard dataset.

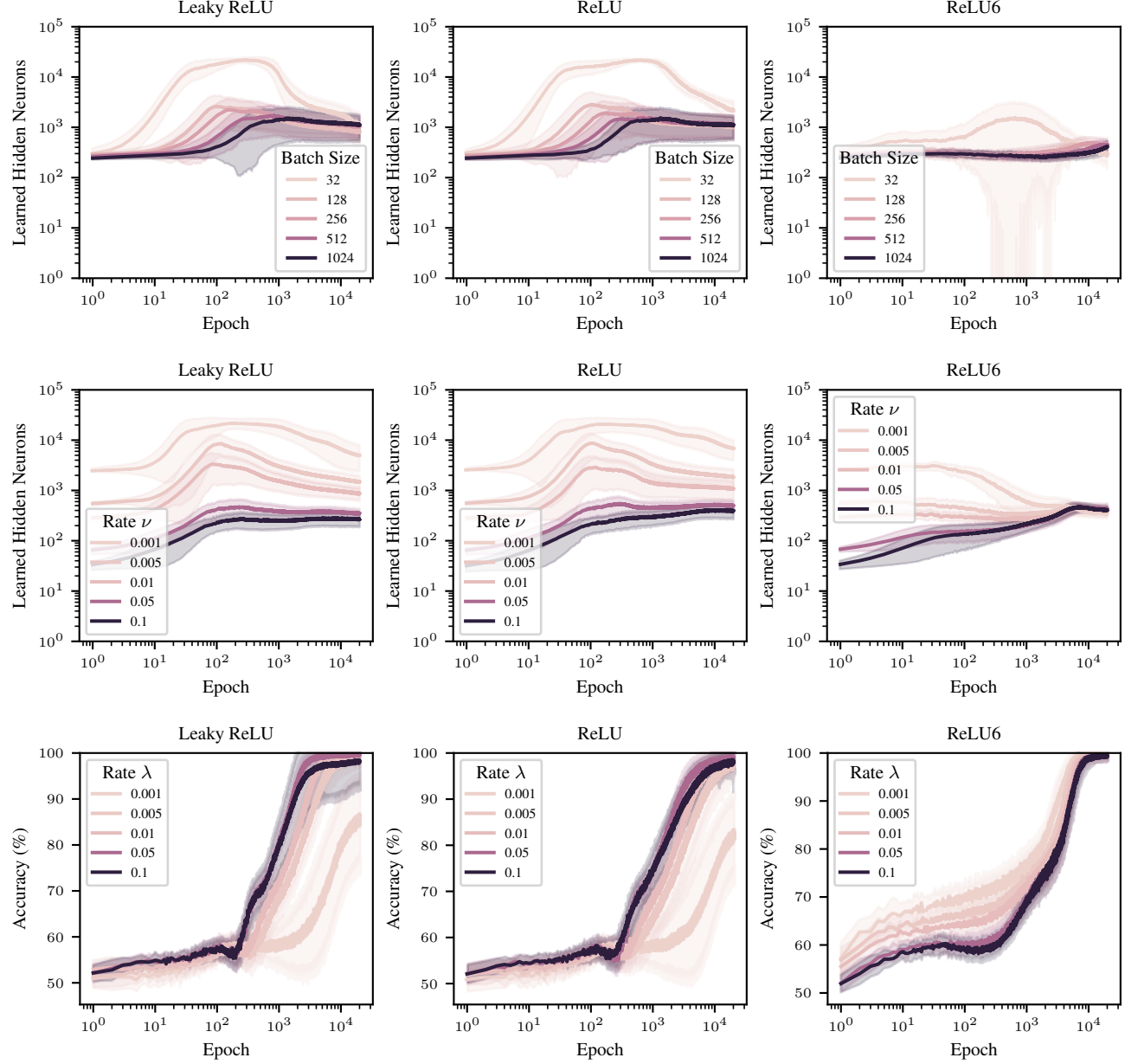


Figure 10. Impact of different batch sizes and starting exponential rates λ , organized by type of non-linear activation function.

These qualitative analyses support our claims that using a bounded activation is one way to encourage the network not to counterbalance the learned rescaling of each neuron. In fact, using a ReLU6 shows a distinctive convergence to the same amount of neurons among all configurations tried. The decreasing trend for LeakyReLU and ReLU activations may suggest that these configurations are also converging to a similar value than ReLU6, but they are taking a much longer time.

G. Learned width for each layer on Graph Datasets

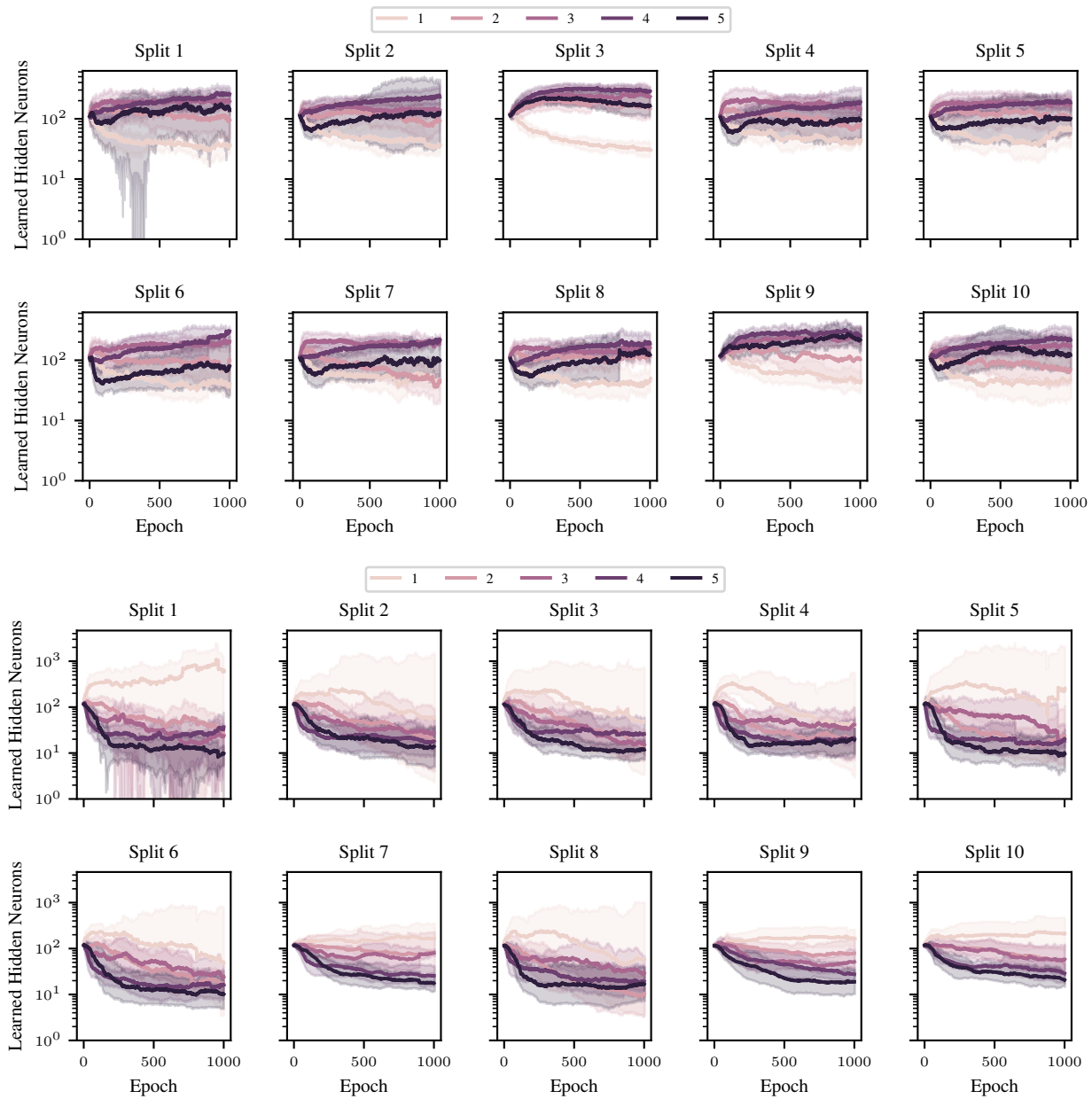


Figure 11. Learned neurons per layer (from 1 to 5), averaged over 10 final runs for each of the 10 best configurations selected in the outer folds. The first and second rows refer to NCI1, the third and fourth refer to REDDIT-B. One can observe similar trends in most cases.